Properties of Confined and Sheared Rhodamine B Films Studied by SFA−FECO Spectroscopy

Anna R. Godfrey Alig, Delphine Gourdon, and Jacob Israelachvili*

Department of Chemical Engineering, University of California, Santa Barbara, California 93106

Received: February 14, 2005; In Final Form: October 24, 2006

We have used a surface forces apparatus and multiple beam interferometry to measure the absorbance of thin films of rhodamine B in water/ethylene glycol solutions while applying and measuring normal and lateral (shear) forces. Both normal and shear forces induced changes in the absorption spectra indicating a change in molecular alignment, and rhodamine−rhodamine and rhodamine−surface interactions. We also measured differences in the absorbance spectra in different regions of the contact indicating, as expected, that the stresses are not uniform throughout the contact area. We also observed crystallization (solidification) parallel to the shearing direction.

I. Introduction

A. Optical Properties of Rhodamine B in Aqueous Solutions. Rhodamine B is commonly used in tunable dye lasers as well as a label in fluorescent measurements. It is well-known that it has different molecular forms which depend on the pH and concentration of the solution,[1−12] and that it readily forms dimers in aqueous solution.[1,3,5,13−23] Shown in Figure 1 are the most prevalent monomer and dimer forms. It is generally agreed that in a neutral solution both the cationic and zwitterionic forms of the dye are present and that both forms dimerize at high concentrations.[5,7,8,10−12,16,24−26] The absorbance spectra of the cationic and zwitterionic monomers are very similar at neutral pH and can be distinguished by adding a small amount of acid or base to the solution.

As shown in Figure 1a,b, the rhodamine B molecule has a planar xanthene base with a carboxyphenyl group that is perpendicular to the base. The transition moment of the dye is parallel to the long axis of the xanthene molecule as shown by the dashed lines in Figure 1a,b. The phenyl group is able to rotate around the phenyl−xanthene bond, and the carboxyl group can rotate around the C−C bond. The surface area of the dye as determined from surface coverage experiments is about 150−160 Å,[2,27−30] and the apparent molecular radius of the dye is 6−8 Å.[31−34] The dimers that form are either H-dimers, which have a sandwich-type head-to-head structure as shown in Figure 1c, or J-dimers, which are known to have an oblique head-to-tail structure (Figure 1d), or tilted parallel structures with a tilt angle less than 54.7° (Figure 1e).[10,35−39] It is not completely understood what interactions occur between the monomer groups to form the dimers, but it is believed that in the cationic H-dimers the carboxy group of one monomer interacts with the oxygen of the xanthene in the other monomer.[3,40,41] According to simple exciton theory,[17,18,42] the sandwich-type H-dimer structure causes a blue shift in the absorbance spectrum. A theoretically possible "linear" structure causes a red shift.[43] The oblique and tilted J-dimers cause a bimodal splitting in the absorbance spectrum with the lower energy peak being more intense.[5,17−19,35−39,42,44,45] If there is a twist angle between the two monomers in the H-dimer, there will be a small peak that is red-shifted relative to the monomer absorbance which accompanies the main blue-shifted peak, again resulting in a

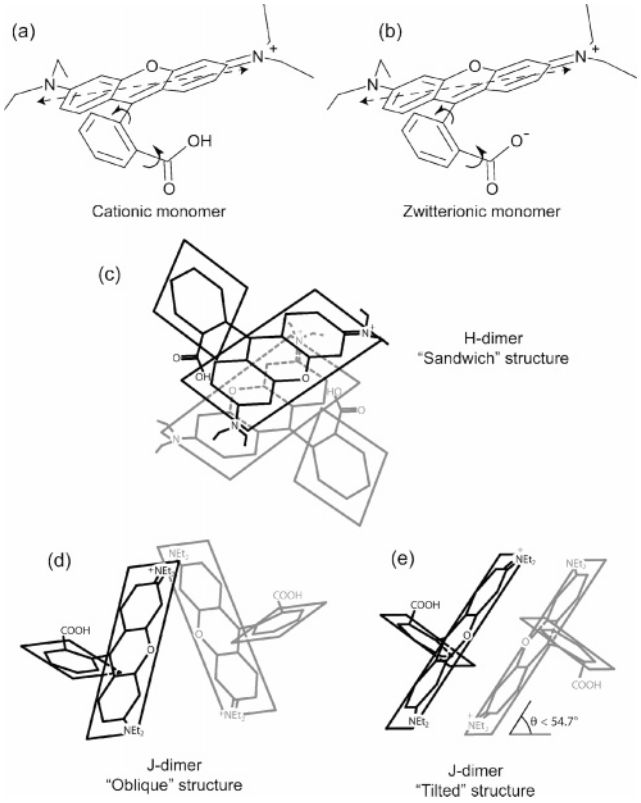

Figure 1. Different monomer and dimer forms of the rhodamine B dye molecule. The transition moment of the dye is indicated by the dashed line in parts a and b, and the rotational bonds are indicated with curved arrows. **(**a**)** Cationic monomer form. **(**b**)** Zwitterionic monomer form. **(**c**)** Schematic of the head-to-head H-dimer (sandwich) configuration constructed from two cationic monomer units. **(**d**)** Schematic of the head-to-tail oblique J-dimer configuration constructed from two cationic monomer units. **(**e**)** Schematic of the tilted J-dimer configuration constructed from two cationic monomer units with a tilt angle <54.7°. All dimers can also be constructed from two zwitterionic monomer units.

* To whom correspondence should be addressed. E-mail: jacob@engineering.ucsb.edu.

10.1021/jp050783g CCC: $37.00
Published on Web 12/10/2006

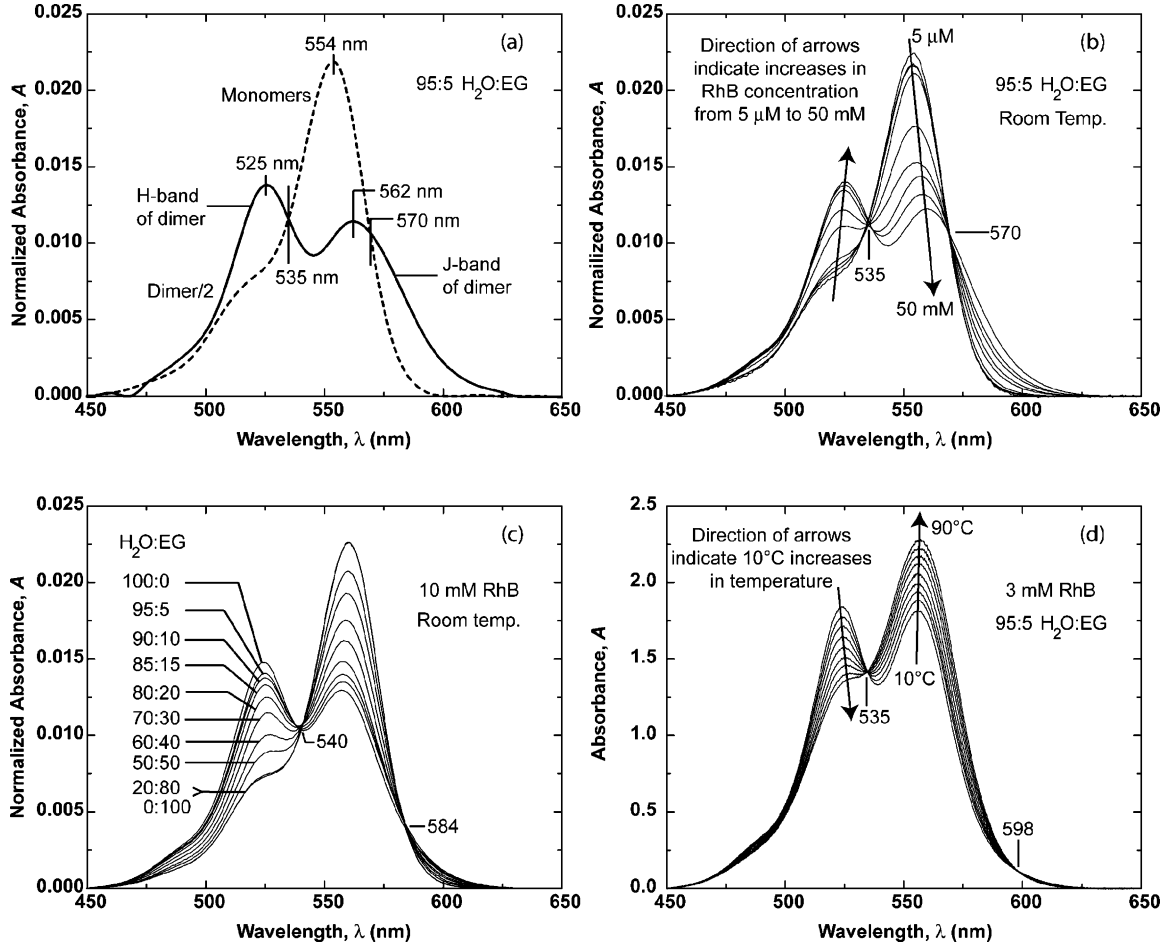

Figure 2. Bulk absorbance spectra. In the case that the path length is unknown, the absorbance has been normalized by the area under the curve in the visible region. **(**a**)** Derived spectra for the monomer (dashed curve) and dimer (solid curve) in a 95:5 volume ratio of water/ethylene glycol (H_2O/EG). The dimer absorbance (dimer/2) has been divided by 2 since it is the spectrum due to the combination of two monomers. **(**b**)** Dependence of the absorbance on RhB concentration in 95:5 H_2O/EG at room temperature. The RhB concentration was increased from 5 μM to 50 mM. Directions of the arrows indicate an incremental increase in concentration by a half order of magnitude. **(**c**)** Dependence of the absorbance of a 10 mM solution of RhB on varying ratios of H_2O/EG solvent at room temperature. **(**d**)** Temperature dependence of the absorbance of a 3 mM solution of rhodamine B in 95:5 H_2O/EG in a 0.1 mm path length cuvette. The temperature was increased from 10 to 90 °C. The directions of the arrows indicate 10 °C increments in temperature.

bimodal splitting but now with the higher energy peak being more intense.

Shown in Figure 2a are the monomer spectra, and the higher and lower energy peaks (or bands) which make up the dimer spectra as determined from our bulk absorbance measurements at different rhodamine B concentrations (Figure 2b). We explain the procedure for determining these spectra in section IIIA. Since the carboxyl/carboxylic acid groups are not a part of the chromophoric unit of the xanthene molecule, the spectra of the zwitterionic and cationic monomers are very similar.

It is known that the addition of alcohols such as ethanol and ethylene glycol helps prevent the formation of aggregates.[7,14] This is thought to be due to a dependence on the solvent dielectric constant or to the hydrophobic/hydrophilic balance of the rhodamine B molecules.[10,20,35,36,38,46,47] The dependence of the absorbance of a 10 mM solution of rhodamine B in varying ratios of water to ethylene glycol is shown in Figure 2c. The spectrum shifts from a monomer structure in pure ethylene glycol (0:100 curve), as in Figure 2a, to a mixed monomer/dimer structure in pure water (100:0 curve).

Temperature also has an effect on the aggregation of rhodamine B in aqueous solutions. The effect of increasing the temperature is similar to the effect of diluting the solution and/or to increasing the ethylene glycol content,[48] as can be seen by comparing parts b−d of Figure 2.

B. Aims of the Experiments. Since the absorbance spectra of rhodamine B and its different forms are so rich in information, we decided to use it as a probe to gain a better understanding of what structural, orientational, and possible temperature changes occur at a shearing interface between two surfaces. It is difficult to find noninvasive methods to study what is actually occurring at a shearing interface. It has been predicted that at the local (molecular) level the temperature rise at a shearing interface can be as high as 1000 °C.[49,50] There is currently no satisfactory method to experimentally determine what the local temperature change actually is. A simple thermocouple cannot measure what the local temperature changes are because it is too large to fit between the surfaces during shearing without affecting the shearing mechanism, and IR detectors cannot resolve better than ∼1 μm. It was hoped that measuring the changing absorbance spectrum of the dye would enable us to probe the temperature changes occurring at the shearing interface at the molecular level.

It is also difficult to unambiguously determine how the orientation of molecules in thin films is affected by the normal and lateral forces between the surfaces under static and dynamic

conditions. There has been some work in which alkane films were frozen during shearing, then freeze-fractured and imaged by atomic force microscopy (AFM) to determine if shear alignment occurs.[51] These experiments allow us to have an idea of how prolonged shear can affect the alignment of certain molecules, but it would be better to find a technique where one can monitor what is happening in situ.

Our specific aims in this paper were to measure the absorbance of thin films under static and dynamic confinement while applying and measuring the normal and shear forces. We review a rigorous method for obtaining the absorbance spectra of the confined films, and we also present a simplified method for measuring changes in the optical properties of the films. We correlated the changes in the optical spectra to changes in the molecular orientation and interactions, surface effects, temperature effects, and shear-induced phase transitions (e.g., solidification).

II. Experimental Section

A. Materials. Rhodamine B (RhB) was used as received from Sigma. Ethylene glycol was purchased from Fluka and was filtered prior to the SFA experiments. Water was used from a MilliQ water system. The muscovite mica used was grade 1 mica, purchased from S & J Trading (Glen Oaks, NY).

Aqueous solutions of RhB in the SFA were varied from 3 to 10 mM in a 95:5 volume ratio of water to ethylene glycol. Ethylene glycol (EG) was added to help prevent aggregation. Solutions used in the bulk spectrophotometric measurements were (1) 1 μM to 50 mM RhB in a 95:5 H_2O/EG solution at room temperature to determine the concentration dependence of the absorbance spectra; (2) 10 mM RhB in 100:0 to 0:100 H_2O/EG solutions at room temperature to determine the EG dependence of the absorbance spectra, and (3) a 3 mM RhB solution in 95:5 H_2O/EG from 10 to 90 °C to determine the temperature dependence.

B. Bulk Spectrophotometric Measurements. Bulk absorbance was measured using a P. General TU-1901 double-beam UV−vis spectrophotometer (GenTech Scientific, Inc., Arcade, NY). Disposable plastic (methacrylate) cuvettes were used for the dilute concentrations. For high RhB concentrations, drops were squeezed between glass cover slips or between two mica sheets. We also used a sealed 0.1 mm path length optical glass cuvette to measure the absorbance of a 3 mM solution at various temperatures. For temperature control, the cuvette was placed between plates that were cooled or heated with a circulating water system from a thermostatted water bath.

C. SFA−FECO Technique. *Surface Forces Apparatus (SFA).* We measured normal and lateral (shear) forces using a surface forces apparatus (SFA Mk III and SFA 2000)[52] while using multiple beam interferometry to obtain fringes of equal chromatic order (FECO).[53,54] In the SFA, films are confined between two crossed cylindrically curved molecularly smooth mica sheets of radii $R \sim 2$ cm. Light is passed through the sheets, where it is reflected back and forth across the trapped film by silver layers on the backsides of the mica sheets. The interference of the light across the film and mica sheets creates FECO which are used to monitor the thickness, uniformity, refractive index, and absorbance (see next section) of the film in situ. The RhB solutions were injected as droplets between the two curved mica surfaces where they remained trapped by capillary forces during the experiments.

The upper surface was mounted on a friction sensing device[55] which uses semiconductor strain gauges to measure the lateral forces caused by the shearing motion of the bottom surface. The bottom surface was sheared against the upper surface using a piezoelectric bimorph slider.[56] The back and forth shearing can be sinusoidal or triangular where, in the latter, the velocity is the same ($\pm V$) over the whole shearing distance.

In order to analyze the intensity of the FECO, pictures of the FECO were recorded using a CCD camera (Roper Scientific MicroMax 1317K). The grating in the spectrometer was gradually adjusted such that pictures were taken over the whole visible spectrum. Each picture covers a wavelength range of about 30 nm and overlaps portions of the adjacent pictures.

FECO Absorption Spectroscopy. In FECO absorption spectroscopy, one takes advantage of the difference in the intensities of the even and odd order interference fringes when an absorbing medium is present between the mica surfaces.[28,57] Using FECO simultaneously with absorption measurements allows one to simultaneously measure absorbance and other important properties of trapped films, such as the film thickness and refractive index, and the contact area which in turn gives the pressure. However, this versatility is at the expense of the maximum efficiencies that could be achieved if each method were to be used (and optimized) separately.

Mächtle et al.[28] derived approximate equations to describe the difference in the transmissions of the even and odd order fringes. We present only their results. If we consider a Fabry−Pérot interferometer with a very thin reflecting and absorbing layer with a refractive index of n-$i\kappa$ and a thickness D at the center of the cavity, we obtain the following expression for the transmission coefficient T of the odd fringes

$$\left|\frac{T(D)_{\text{odd}}}{T(0)_{\text{odd}}}\right|^2 = 1 - \frac{2\pi D}{\lambda_m{}^0}\frac{2n\kappa}{n_{\text{mica}}}\left(\frac{1-r_1}{1+r_1}\right) \approx 1 \text{ for } m \text{ odd} \quad (1)$$

where $T(D)$ is the transmission coefficient of the absorbing film of thickness D, $T(0)$ is the transmission coefficient without the film ($D = 0$), r_1 is the reflection coefficient of the silvered mica/substrate interface, n_{mica} is the refractive index of mica, and $\lambda_m{}^0$ is the wavelength of the m-order fringe. When $D < 6$ nm ($D < 0.01\lambda_m{}^0$) and $r_1 \approx 1$, both $2\pi D/\lambda_m{}^0$ and $(1 - r_1)/(1 + r_1)$ in eq 1 are very small. Therefore, the transmission (intensity) of the odd order fringes $T(D)_{\text{odd}}$ is changed very little due to the absorbing film. In contrast, the transmission (intensity) of the even order fringes $T(D)_{\text{even}}$ is decreased significantly by the absorbing film, as given by

$$\left|\frac{T(D)_{\text{even}}}{T(0)_{\text{even}}}\right|^2 = \left[1 + \frac{2\pi D}{\lambda_m{}^0}\frac{n\kappa}{n_{\text{mica}}}\left(\frac{1+r_1}{1-r_1}\right)\right]^{-2} \text{ for } m \text{ even} \quad (2)$$

In eq 2, the small value of $2\pi D/\lambda_m{}^0$ is offset by the large $(1 + r_1)/(1 - r_1)$ term (since $r_1 \approx 1$) which allows the transmission of the even fringes to be substantially reduced. Figure 3a shows the fringes for mica−mica contact in air where there is no absorbing between the surfaces ($D = 0$). The odd fringes are those that appear sharp at the (upper) edge while the even fringes appear more rounded; but both are equally bright. Because mica is birefringent, it splits the incoming beam (whether unpolarized or polarized) naturally into the two polarization directions determined by the crystallographic axes of the mica sheets. Thus, each fringe appears as a doublet, thereby also allowing for simultaneous measurements to be made on these two components. (One can predetermine these directions by mounting the mica sheets with their crystallographic axes along, say, the shearing direction and/or the "twist" angle of the two lattice axes relative to each other.)

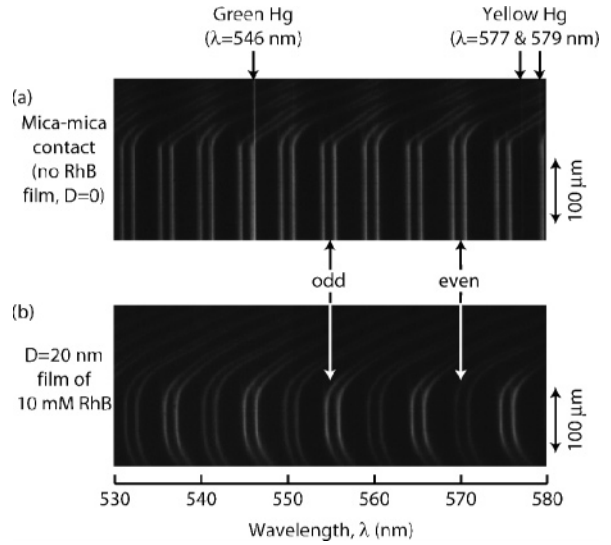

Figure 3. (a) FECO spectrogram for mica−mica contact ($D = 0$) and (b) when confining a 10 mM solution of rhodamine B in a 95:5 H_2O/EG film of thickness $D = 20$ nm. In part a, due to the strong adhesion in air, the odd fringes have sharp edges while the even fringes have rounded (or less sharp) edges. The green and yellow Hg lines are used to calibrate the wavelength of the fringes. When the absorbing RhB film is confined between the mica surfaces (b), the odd fringes remain bright while the even fringes appear dark. Due to the lack of adhesion, both order fringes have rounded edges.

As predicted by eqs 1 and 2 above, when RhB (or any other absorbing medium) is present between the mica surfaces, the odd fringes remain bright while the even fringes appear dark (Figure 3b). By comparing the intensities of the even and odd fringes, one can determine the absorption spectrum of the film.

III. Results and Discussion

A. Derivation of the Dimer Spectrum. The dimer spectrum shown in Figure 2a was derived from the bulk solution spectra shown in Figure 2b, which shows that as the RhB concentration is increased from 5 μM to 50 mM, the higher wavelength peak (main peak) at ~554 nm decreases and the lower wavelength peak at ~525 nm increases. The increase in the lower wavelength peak indicates an increase in H-dimer (and possibly even higher *n*-mer) concentration. It can be assumed that at low concentrations only monomers are present in the solution. The isobestic points at 535 and 570 nm indicate that there is a reaction equilibrium between the different species of the RhB dye. The equilibrium between the monomers and dimers in the solution may be written as

$$\text{monomer} + \text{monomer} \leftrightarrow \text{dimer} \tag{3}$$

with an equilibrium constant K which follows the law of mass action. Accordingly, K can be described as a function of the monomer fraction, x, and the solution concentration, c:

$$K = \frac{2x^2c}{1-x} \tag{4}$$

The absorption spectrum of the mixed monomer/dimer solution, $A_{solution}$, depends on the monomer and dimer spectra as follows

$$A_{solution} = A_m x + A_d \frac{1-x}{2} \tag{5}$$

where A_m is the absorbance of the monomer (assumed to be equal to the low concentration bulk spectrum) and A_d is the bulk absorbance spectrum of the dimer. Unfortunately, we cannot determine the spectra of the H- and J-dimers separately, and we therefore treat them as a single generic dimer. The absorbance of the dimer is then determined by trial and error by guessing a value for K, which should apply at all concentrations, then determining x for each concentration at a fixed solvent composition (95:5 H_2O/EG) and room temperature, and calculating A_d until an A_d is found that is consistent at all concentrations.[9,19−21,45,58] The dimer spectrum determined in this way is shown in Figure 2a, which exhibits two peaks which are labeled as the H- and J-bands.

B. Static Structure of the Confined Dye. To rigorously determine the absorption spectra of the thin dye films from the FECO, one needs to specifically determine the imaginary part of the refractive index, κ. As seen in eqs 1 and 2 above, the imaginary refractive index is coupled with the real part of the refractive index, n. In order to decouple the real and imaginary parts of the refractive index we need to also consider the resonance condition for even fringes[28,57]

$$(n^2 - \kappa^2)D = \frac{m\Delta\lambda_m n_{mica}}{2} \text{ for } m \text{ even} \tag{6}$$

where $\Delta\lambda_m$ is the shift in the wavelength of the fringe relative to its position in mica−mica contact ($D = 0$).

As discussed by Helm and co-workers,[28,57,59] the shape of the peaks due to the transmission of the FECO as a function of the wavelength can be fitted with Lorentzian curves (height × full width half-maximum × $\pi/2$). It is also helpful to consider the transmitted intensity, I_0, rather than the transmission coefficient, T, using the following relation

$$I_0 = |T|^2 I_i \tag{7}$$

where I_i is the incident intensity. After substituting the Lorentzian relation and eq 7 into eqs 1 and 2, we get the following equations for the odd and even FECO

$$\frac{I_{odd}}{I_i} = \frac{\pi}{2} W_{odd} \tag{8}$$

$$\frac{I_{even}}{I_i} = \frac{\pi}{2} W_{even}\left[1 + \frac{2\pi D}{\lambda_m^{\,0}} \frac{n\kappa}{n_{mica}}\left(\frac{1+r_1}{1-r_1}\right)\right]^{-2} \tag{9}$$

where W is the full width at half-maximum of the peak. The full width half-maximum of the peak can be related to the reflection coefficient by[28,57]

$$W_{odd} = \frac{\lambda_m^{\,0}(1-r_1^{\,2})}{m\pi r_1} = \frac{\lambda_m^{\,0}(1-r_1)(1+r_1)}{m\pi r_1} \tag{10}$$

Using eqs 8−10, we can obtain the following equation for the real part of the refractive index:

$$n = \frac{mn_{mica}}{2\kappa D} \frac{r_1}{(1+r_1)^2}\left[\left(\frac{I_{odd} W_{even} W_{odd}}{I_{even}}\right)^{1/2} - W_{odd}\right] \tag{11}$$

Finally, eq 11 can be substituted into eq 6 and rearranged to solve for κ^2

$$\frac{\kappa^2}{C_1} = \frac{-\Delta\lambda_m \pm \sqrt{(\Delta\lambda_m)^2 + 4C_2^{\,2}}}{2} \tag{12}$$

where

$$C_1 = \frac{mn_{\text{mica}}}{2D} \tag{13}$$

and

$$C_2 = \frac{r_1}{(1+r_1)^2}\left[\left(\frac{I_{\text{odd}}W_{\text{even}}W_{\text{odd}}}{I_{\text{even}}}\right)^{1/2} - W_{\text{odd}}\right] \tag{14}$$

To compare the confined film absorbance spectra to the bulk absorbance spectra, we use the fact that the absorbance, A, is proportional to the imaginary refractive index scaled by the wavelength:

$$A \propto \frac{\kappa}{\lambda} \tag{15}$$

As seen in eq 12, the imaginary refractive index calculated at each even fringe is sensitive to the shift in the wavelength of the FECO as well as the width of the surrounding even and odd fringes. This means that to obtain very accurate or even reasonable measurements of the imaginary refractive index it is critical that both the wavelength and Lorentzian fits of the FECO be very accurate.

Figure 4a shows the fringes across the whole visible spectrum of a 10 mM solution of RhB in a 95:5 water/ethylene glycol film of thickness $D = 14$ nm. An average intensity taken through the flat portion of the fringes enables us to plot the intensity, I, versus the wavelength, λ, as shown in Figure 4b. In the region from about 500 to 600 nm, the intensity of the even fringes (envelope shown by the dashed line) is clearly lower than that of the odd fringes (envelope shown by the solid line), while at higher and lower wavelengths the intensities are about the same. The overall shape of the envelope of the maximum intensity is due to the output of the lamp, the absorbance of the silver reflecting layer, the absorbance of any lenses or mirrors in the path length of the light, and the sensitivity of the CCD camera.

To determine the absorbance, A, of the film using the above-described rigorous method, each peak in Figure 4b was fitted with a Lorentzian curve to obtain its integrated intensity (the area under each peak), its full width half-maximum, and the wavelength at its center. The imaginary refractive index, κ, was calculated for each even fringe using eq 12, where the values for the I_{odd} and W_{odd} were calculated as the average of the two neighboring odd fringes. Thus, to find κ for the mth even fringe, the values for I_{odd} and W_{odd} are calculated as follows:

$$I_{\text{odd}} = \frac{I_{\text{odd},m-1} + I_{\text{odd},m+1}}{2}$$

$$W_{\text{odd}} = \frac{W_{\text{odd},m-1} + W_{\text{odd},m+1}}{2} \text{ where } m \text{ is even} \tag{16}$$

The even fringe is compared to the two odd fringes on either side of it to normalize the effect of the curvature of the intensity envelope. The film thickness, D, is determined by using odd fringes in the wavelength region between the green and yellow Hg lines where our wavelength readings are the most accurate. Figure 4c shows the resulting absorbance spectrum (κ/λ) of the (statically) confined RhB film, which was constructed from the fringes and intensity spectrum of Figure 4a,b. Also shown is the absorbance curve of the same bulk solution measured using the spectrophotometer. For ease of comparison, the curves have been normalized by their areas in the visible region.

As mentioned earlier, the method of using eq 12 to calculate the absorbance of the spectra depends very sensitively on the shifts, widths, and locations of the FECO fringes. In the interferometric method, the thicker the mica, the more FECO there are present in the visible range which increases the number of points that can be used to construct the absorbance curve. On the other hand, if the FECO are very close to each other, it is difficult to have a very accurate measure of both the change in the location and width of each fringe. In fact, if the fringes are too close together, the resolution can become so bad that the shift in the wavelength in some regions can appear to shift to lower wavelengths ($\Delta\lambda_m < 0$) which results in unreasonable values for the imaginary and real parts of the refractive index. As a result, we found that it can often be more reasonable and valuable to calculate the ratio of the intensity of the even fringes compared to the odd fringes and treat this as our absorbance

$$A(\lambda_m) = -\ln\left[\frac{2\int I_m \, d\lambda_m}{\int I_{m-1}\, d\lambda_{m-1} + \int I_{m+1}\, d\lambda_{m+1}}\right], \text{ for } m \text{ even} \tag{17}$$

where λ_m is the average wavelength of the even fringe. It is not actually correct to call this the absorbance because it does not take into account the effect of both the imaginary and real parts of the refractive index on the intensity of the even fringe (cf. eq 9). Nonetheless, in this paper we will still refer to this value as the absorbance of the film on the basis of the simple definition of the absorbance

$$A = -\ln\frac{I_0}{I_{\text{i}}} \tag{18}$$

where I_{i} is the incident intensity and I_0 is the transmitted intensity. Figure 4c shows the absorbance curve, $-\ln(I_{\text{even}}/I_{\text{odd}})$, of the (statically) confined RhB film, which was constructed from the fringes and intensity spectrum of Figure 4a,b using eq 17.

As seen in Figure 4c, the rigorously calculated absorbance spectrum (curve κ/λ, eq 15) of the confined film is very similar to the simply calculated absorbance spectrum (curve $-\ln[I_{\text{even}}/I_{\text{odd}}]$, eq 17). In most of our analysis, we therefore compare changes in the transmitted intensity using the simplified absorbance spectra, even though the authors recognize that this is not the most rigorous method. In some situations we were able to rigorously calculate the absorbance spectra and found that the final conclusions were unchanged from those where we used the simplified formula.

As shown in Figure 4c, the higher wavelength peak (main peak) of the static absorbance spectrum of confined RhB films at 580 nm is red-shifted relative to the main peak of the bulk solution (at 558 nm) by about 22 nm. Also, in the confined RhB film, the lower wavelength "peak" is more of a shoulder than the peak found in the bulk solution. It has been shown that the absorption spectra of xanthene dyes in clay suspensions are red-shifted relative to the monomer spectra.[14,46,60−65] Specifically, Grauer et al.[60] found red shifts of 13 and 10 nm for RhB on montmorillonite and Laponite surfaces, respectively. López Arbeloa and co-workers studied the absorption and intercalation of rhodamine 3B in various clays and found red shifts of the monomer absorption maximum of 7, 12, and 12.5 nm on montmorillonite,[46] 10, 17, and 23 nm on Hectorite,[65] and 10 nm on Laponite[66] (a synthetic Hectorite). In montmorillonite and Hectorite the smaller shifts were attributed to monomer absorption on the external clay surface, the intermediate shifts were attributed to monomer adsorption in the interlamellar regions, and the larger shifts were attributed to dimers or higher

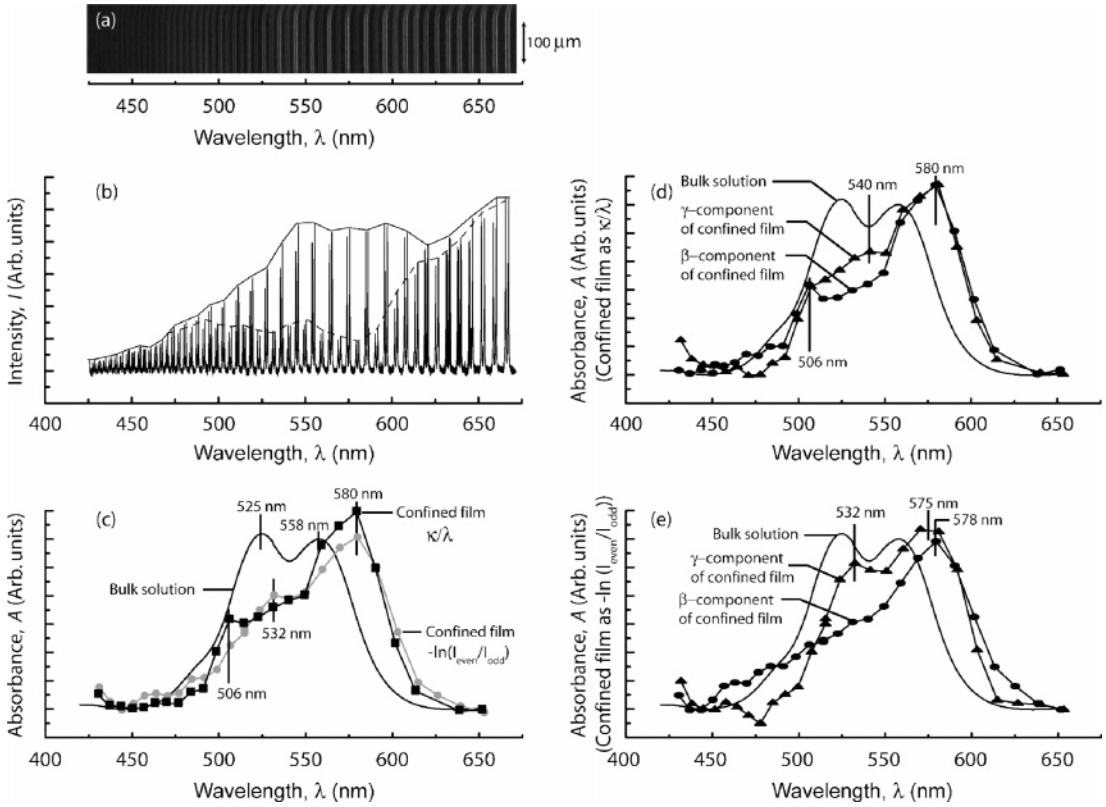

Figure 4. **(a)** FECO spectrogram of a confined 10 mM RhB solution in 95:5 H_2O/EG of thickness $D = 14$ nm. **(b)** Intensity, I, as a function of wavelength, λ, averaged over a cross section of the flat portion of the fringes in panel a. The maximum intensity of the odd fringes is shown by the solid envelope, and the maximum intensity of the even fringes is shown by the dashed line envelope. The region from about 500 to 600 nm shows the most contrast between odd and even order fringes, since this is where the confined dye has the highest absorbance. **(c)** Absorbance, A, as a function of wavelength of the bulk solution (—), the confined film (—■—) calculated as κ/λ, and the confined film (—●—) calculated as $-\ln(I_{even}/I_{odd})$. The absorbance of the confined film (κ/λ) was determined from the intensity of panel b via eqs 12−15 while the absorbance of the confined film, $-\ln(I_{even}/I_{odd})$, was determined from the intensity of panel b via eq 17. All spectra were normalized by the area below them for ease of comparison. The peak at 558 nm is the main peak of the bulk solution which is a mix of the dimer at 562 nm and the monomer at 554 nm (see Figure 2a). **(d)** Absorbance spectra of the bulk solution (—), the β-component of the confined film (—●—), and the γ-component of the confined film (—▲—). The absorbance spectra of the β- and γ-components of the confined film were calculated as κ/λ using eqs 12−15. **(e)** Absorbance spectra of the bulk solution (—), the β-component of the confined film (—●—), and the γ-component of the confined film (—▲—) The absorbance spectra of the β- and γ-components of the confined film were calculated as $-\ln(I_{even}/I_{odd})$ using eq 17.

aggregates. Grauer et al.[61] studied the adsorption and intercalation of rhodamine 6G in montmorillonite and Laponite and found red shifts of 20 and 13 nm, respectively. Tapia Estévez and co-workers studied the adsorption and intercalation of rhodamine 6G and found red shifts of 3, 19, and 29 nm in Hectorite,[64] and 11 and 24 nm in Laponite,[62,63] where the smallest shifts (<19 nm) were attributed to external monomers, shifts of 19−24 nm to internal monomers, and the 29 nm shift to an external dimer. Conversely, Sasai et al.[67] found no wavelength shift when they studied the intercalation of rhodamine 6G in a fluor-taeniolate.

The adsorption of the dye in clay systems has generally been attributed to ion exchange,[40,41,46,60,61,63−70] though Yariv has determined that the dye molecules adsorb in excess of their cation exchange capacity.[71] The red shifts have been attributed to a change in the polarity of the environment of the dye as it goes from an aqueous phase to the more polar solid clay phase,[1,37,46,60−62,71] although the reduced dielectric constant at a clay surface may be the cause, which would be consistent with the red shifts observed in lower dielectric constant ethylene glycol/water solutions and at higher temperatures. The red shift of the main peak could also indicate the presence of the J-dimer which is not present in the bulk aqueous solution except at very high concentrations. It has been reported that J-dimers have a specific preference to adsorb to surfaces.[27,37,72] Red shifts in the absorbance spectra of RhB films have also been found on surfaces such as glass (∼13 nm),[37,73] silica gel (∼8 nm),[10,36,38,74] ZnO (∼8 nm),[29] indium oxide (∼13 nm),[73] and quartz (∼6 nm),[30] as well as on arachidic acid monolayers (∼11 nm).[75]

In the confined films in the SFA, it appears that the intensity of the absorbance of the lower wavelength peak is much lower than that in bulk solutions at the same concentration (Figure 4c). This could be due to a larger percentage of monomers and/or J-dimers in the confined film. Molecular models have shown that J-dimers are the most energetically favorable dimer found on the external surfaces of montmorillonite in concentrated solutions.[69] We therefore believe that the red shifts in the peaks and the decrease in intensity of the lower wavelength peak indicate the presence of mainly monomers and J-dimers in the confined films.

Orientation Effects. The birefringence of mica allows us to see whether any orientational ordering occurs in the confined films. The doublets which appear in the FECO are due to the birefringence of the mica, where the lower wavelength fringe of the doublet is due to the β-component of the refractive index, and the higher wavelength fringe to the γ-component. If the film between the surfaces were completely isotropic, the absorbance spectra of the β- and γ-components would be the same. Shown in Figure 4d,e are the absorbance spectra of the film whose FECO were shown in Figure 4a, where the spectra in part d were calculated using the rigorous method (κ/λ) and in part e using the simplified method, $-\ln(I_{even}/I_{odd})$. In parts d

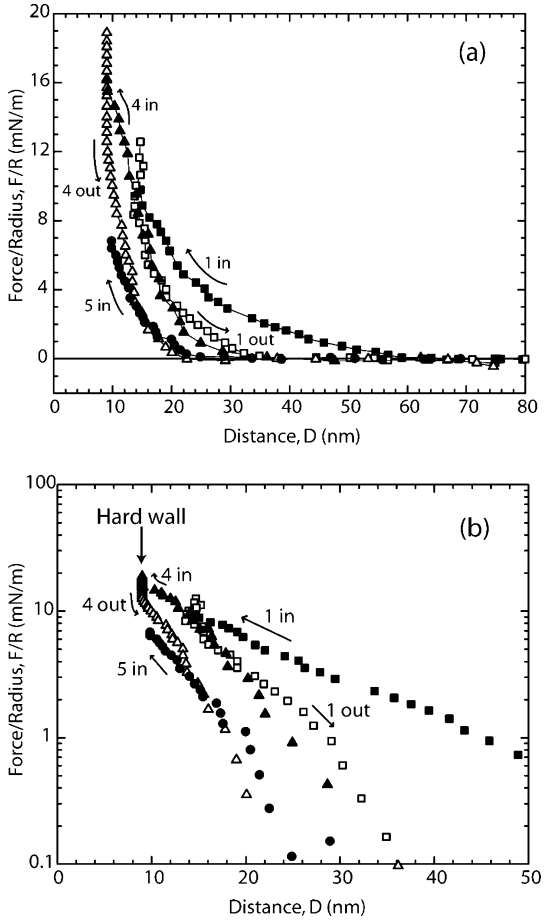

Figure 5. Force runs of 10 mM RhB solution in 95:5 H_2O/EG plotted on **(**a**)** linear and **(**b**)** semilog scales. Zero distance ($D = 0$) is defined as mica−mica contact in dry N_2 gas. Solid symbols and "in" indicate loading, and open symbols and "out" indicate unloading. The numbers refer to the order of the force runs. Runs 2 and 3 "in" and "out" were nearly identical to run 1 "out" and are omitted for clarity.

and e of Figure 4, it is clear that the β- and γ-spectra are different: the γ-component spectra appear to have more prevalent shoulders in the low wavelength region (∼530−540 nm) than the β-component spectra. This shoulder in the γ-component spectra is probably due to absorbed H-dimers where the peak is red-shifted relative to the bulk spectra as a result of the surface adsorption and confinement. Since the β- and γ-component spectra are different, there seem to be some orientation effects, but it is not obvious what that orientation is.

C. Normal Force Measurements. Figure 5 shows normal force measurements between two mica surfaces in a solution of 10 mM RhB in 95:5 H_2O/EG at room temperature. These experiments were carried out to gain a better understanding of the strength of interaction between the adsorbed RhB molecules and the mica surfaces, and the organization of the molecules within the confined films. During the first approach or loading cycle ("1 in" in Figure 5a), repulsive forces were first felt at $D \approx 60$ nm, which were roughly exponential (Figure 5b). The surfaces were then brought together to a separation of about 15 nm. During subsequent approaches and separations the repulsive regime moved inward until, by the fourth compression, a fixed "hard wall" built up at $D = 9$ nm.

The repulsive forces appear to be due to a concentration gradient of RhB aggregates, and the "hard wall" appears to be due to a solidification of this surface layer. Shown in Figure 6 is a schematic of the surfaces after successive loading/unloading

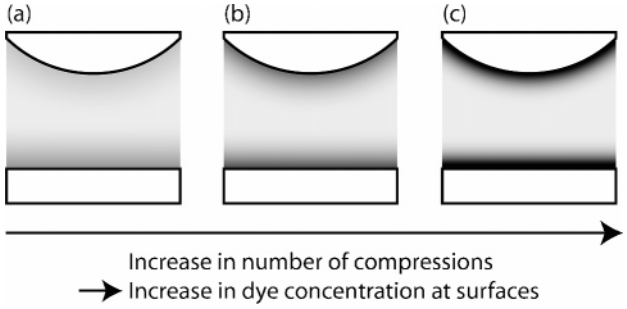

Figure 6. Schematic showing **(**a**)** initial concentration, with a decreasing concentration away from each surface. After the surfaces in part a have been brought close together and separated, the concentration gradient changes more steeply **(**b**)** with a buildup at each surface. In part c, the surfaces have been separated after being brought even closer together than in part b, showing an even higher concentration buildup at the surfaces, and with a sharp decrease in concentration away from the surfaces.

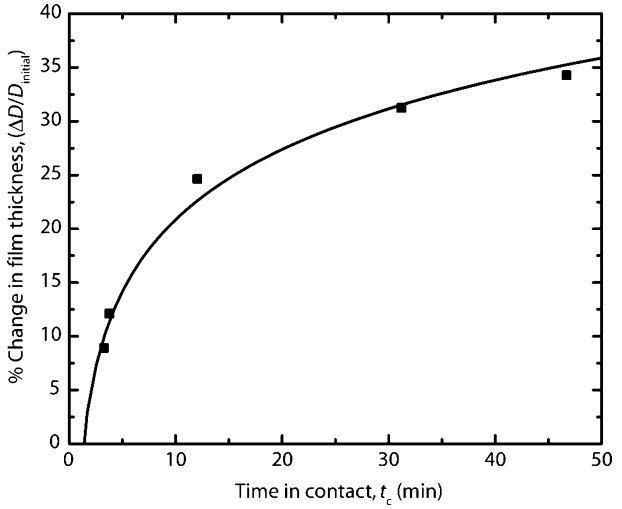

Figure 7. Graph of the percent change in film thickness as a function of time in compressive contact. In all cases, the initial film thickness was between 13 and 16.5 nm. The line is a logarithmic fit to the data. When the initial film thickness was less than 9 nm, the "hard wall" thickness, there was no change with the contact time.

cycles. In Figure 6a, the concentration gradient extending from each surface is initially fairly long ranged (∼ 30 nm). With each successive compression (a → b) the surfaces were brought closer in resulting in a more compressed surface layer and a decrease in the range of the concentration gradient.

If the surfaces were brought together until they reached a film thickness of $D \sim 13-16.5$ nm, and were then kept in place under the same compressive force (or pressure), the film thickness was found to decrease logarithmically with time (Figure 7). This indicates that the RhB molecules were slowly rearranging into a more favorable packing density, although some squeeze out may also be occurring (see later). No further decrease was observed once the film thickness reached 8−9 nm.

Effect of Pressure on the Structure of RhB Films. Using FECO adsorption spectroscopy we simultaneously monitored the absorbance of RhB films, their thickness, and refractive index, as a function of the pressure applied across the films. Figure 8 shows measured FECO and the absorbance spectra of a 10 mM solution of RhB in a 95:5 water/ethylene glycol solution between two mica surfaces. The spectra were recorded as the surfaces were slowly pressed together. Initially (Figure 8a), the surfaces are far from contact, with a $D = 80$ nm thick film between

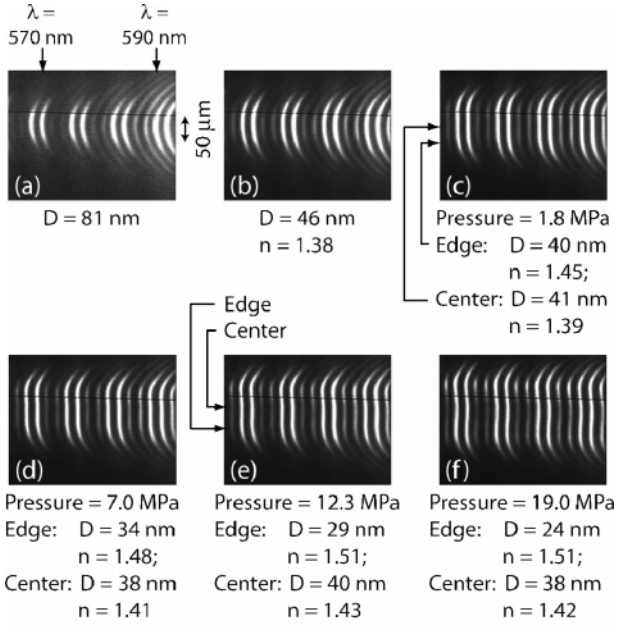

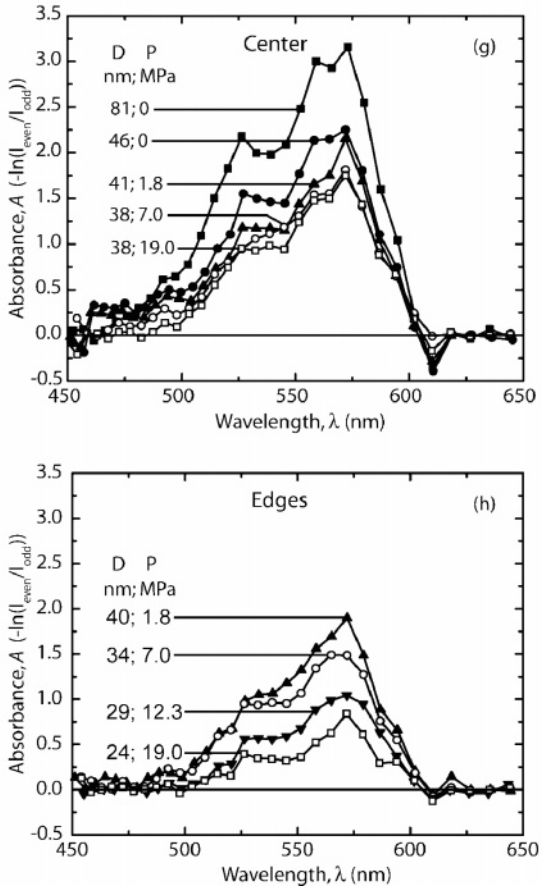

Figure 8. **(**a−f**)** FECO of a 10 mM solution in 95:5 H_2O/EG recorded as the applied normal pressure was increased from 0 to 19 MPa. The surfaces were brought together from $D = 81$ nm (a) until they began to flatten at about 46 nm (b). As the load was further increased, the fringes began to bulge in the center as can be seen at 7.0 MPa (d). The surfaces continued to be pressed together to a pressure of 19 MPa (f). Panel g shows the absorbance spectra recorded at the centers of the contact of the fringes shown in panels (a−f). In part h are the absorbance spectra at the edges of the contact.

them. The film is so absorbing that the even order (doublet) fringes are barely visible, and because of the thickness of the film, even the intensities of the odd (doublet) fringes are affected. Because the intensities of the odd fringes were affected, the intensities of the initial fringes before introducing RhB solution were used as the reference to determine the film's relative absorbance. As the surfaces are brought closer together, the absorbance of the film decreases. Once the film thickness falls below about 40 nm, the fringes bulge inward indicating trapped solution at the center due to elastohydrodynamic effects where the edges of the contact are closer than at the center;[76] and the refractive index of the film (denoted by *n* in parts a−f) is greater at the edges than at the center.

As shown in Figure 8g,h, for the center and edges, respectively, the absorbance decreases as *D* decreases. However, at the center of the contact (part g), the low wavelength peak at ∼525 nm decreases more, while at the edges (part h) the high wavelength peak at ∼570 nm decreases more. In addition, a small peak at 590 nm, which can be attributed to the J-dimer, emerges in the absorbance spectra in both panels, becoming particularly pronounced in the thinnest, highest pressure, 24 nm thick film in Figure 8h.

Throughout the film, with increasing pressure and decreasing film thickness, the refractive index increases as the absorbance decreases. This implies that RhB is being forced out of the contact area but not at the same rate as the film thins; i.e., an immobilized concentrated layer of adsorbed RhB remains attached to the surfaces as the RhB in the remaining solution is squeezed out. This is consistent with our normal force profiles (Figure 5) which indicated that there was a concentration gradient of RhB aggregates with higher concentrations at the mica surfaces, and it is also consistent with the findings of Mächtle et al.[28]

D. Effects of Shear. During shearing we monitored the changing FECO and absorbance spectra while simultaneously measuring the friction (shear) forces. The friction coefficients were high-reaching values of ∼0.6. Both smooth and stick-slip sliding were observed, with transitions between these two modes of sliding that were sometimes correlated with the changes observed in the absorbance, as described below.

Shear-Induced Crystallization and Restructuring. During shearing experiments, we often found that dark bands appeared in the FECO, accompanied by ribbon-shaped regions that formed within the contact area that appear to be crystals. Figure 9a shows the Newton's rings observed when the contact is viewed with a simple microscope from above, and Figure 9b shows the corresponding fringes as seen in the spectrometer. The abrupt disappearance of the bright fringes, only to reappear at some lateral distance away at the same film thickness, shows that these bands are not wear tracks due to damage (see also Figure 10). This phenomenon has also been found in other, similar systems.[77] Initially, the fringes show a slight deformation, but as the shearing continues the deformation transforms into a dark band across the fringes indicating that the film in these areas is too absorbing to allow any light to pass through them. This often causes the fringes to have light and dark bands, which is described further below. If the surfaces are separated at this point, the crystals do not dissolve back into solution.

A more detailed example of a shear-induced deformation is shown in Figure 10 where crystallization is just beginning to form in the film. In this experiment, 10 mM of RhB in 95:5 water/ethylene glycol was injected between the surfaces. The surfaces were then pressed together until they flattened (Figure 10a). Keeping the surfaces under the same normal force, they were then sheared back and forth at 3 μm/s over a distance of 30 μm. The friction was smooth and initially increased to ∼30 mN then decreased (i.e., there was a "stress overshoot" or "shear

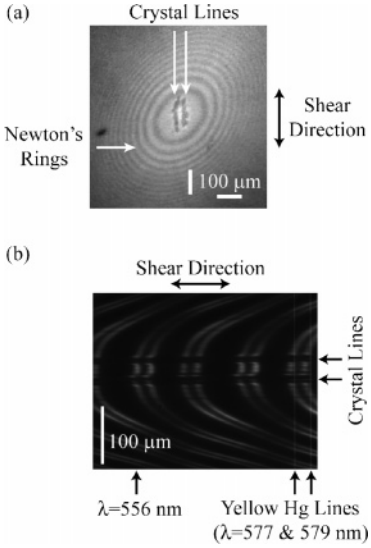

Figure 9. **(**a**)** The Newton's rings as seen from above the contact. In the center of the contact region are two ribbon-shaped regions (dark bands) attributed to crystal formation. These ribbons are oriented parallel to the shear direction as indicated on the figure. In part b are the corresponding FECO.

thinning") to a steady-state value of ∼10 mN; at the same time, the film thickness increased from ∼5 to ∼25 nm (Figure 10b). Interestingly, the reduction in the friction force coincided with the appearance of the partially darkened deformations shown in Figure 10b, but no crystals formed even after sliding for 60 more cycles, i.e., over a total shearing distance of ∼2 mm and over a time of ∼10 min. Figure 10c shows the FECO at the point where the shearing was stopped, and Figure 10d shows the fringes 40 min later. As shown in Figure 10f, the normalized absorbance spectra did not change during the shearing and after stopping.

After purging with dry nitrogen for about 40 h to evaporate the solvent, the film thinned, especially at the edges (Figure 10e), and the absorbance spectra were now blue-shifted by about 20 nm relative to those before drying, with the additional appearance of a peak at 530 nm (Figure 10f). The dark deformed regions behaved similarly, but the 530 nm peak was already evident during the shearing. The increase in this peak indicates an increased fraction of H-dimers, which was also observed on static confinement, as described above.

The changes in the absorbance spectra in the deformed regions indicate a change in the configuration of the molecules during shearing, a shear induced effect that is highly localized within the contact region. The variations in the absorbance of the film at different regions of the contact indicate that not all regions are the same, for reasons discussed by Granick.[78,79]

These blue shifts due to drying cancel the red shift caused by confinement, returning the spectra closer to the bulk solution spectrum (Figure 4c), where the middle of the films seems to most closely resemble the spectrum of pure monomers (Figure 2a).

Correlation between Absorbance Changes and Friction Behavior. Figure 11 shows friction traces in the "transition" regime from stick-slip to smooth sliding (Figure 11, parts a → b). In this experiment an initially 9 nm thick film was sheared back and forth at 0.08 μm/s over a distance of 100 μm. Figure 11c shows the absorbance spectra as measured before shearing, during shearing at the last part of the transition regime (panel a at 120 min), during shearing in the smooth steady-state sliding regime (panel b at 200 min), and after stopping. The main peak

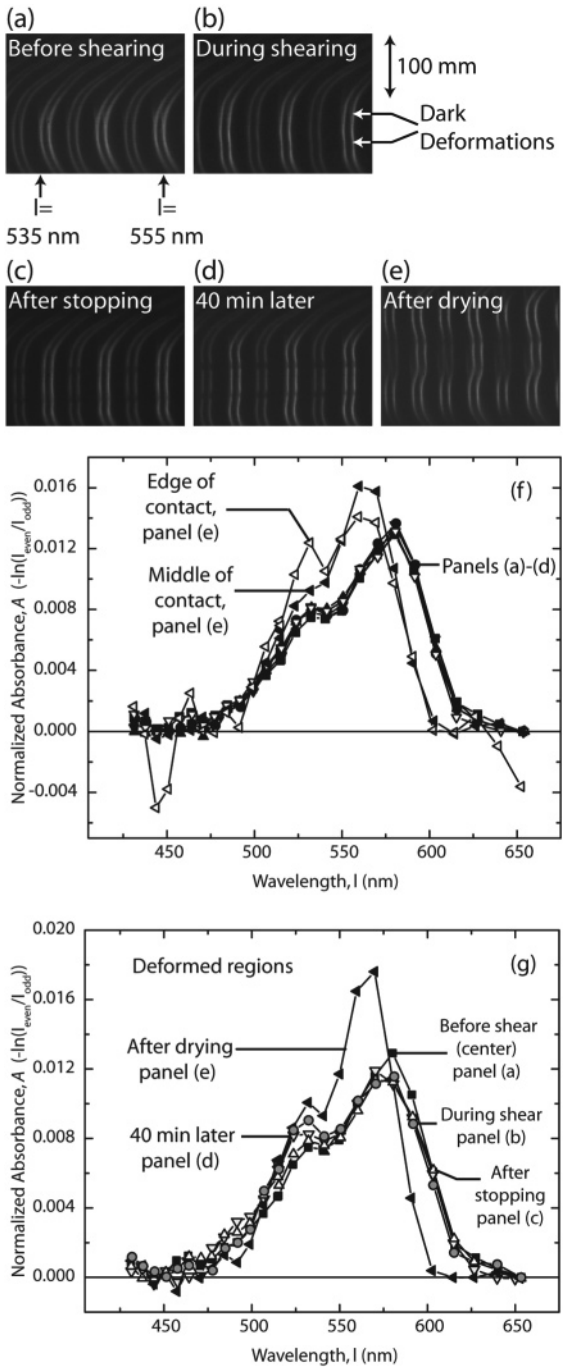

Figure 10. **(**a−e**)** FECO of a 10 mM RhB solution in 95:5 H_2O/EG recorded **(**a**)** before shearing, **(**b**)** during back and forth shearing at 3 μm/s over a distance of 30 μm, **(**c**)** just after stopping shearing over a total shearing distance of ∼2 mm, **(**d**)** 40 min after stopping before the commencement of drying, and **(**e**)** after 40 h of continuous drying by purging with dry nitrogen gas. Before shearing, the fringes are only slightly flattened at the center of the contact (a). During shearing the contact area increased and deformations due to localized accumulation of RhB molecules near the edges of the contact appeared (b). (f) Corresponding absorbance spectra taken before shearing, during shearing at steady state, just after stopping shearing, 40 min after stopping shearing at both the middle and edges of the contact, and after 40 h of drying with dry nitrogen at both the middle and edges. (g) Absorbance spectra of the center of the contact before shearing, and of the deformed regions of the contact during shearing, just after stopping shearing, 40 min after stopping shearing, and after 40 h of drying.

of the absorbance spectra shifted from about 580 nm to about 565 nm while shearing in the steady-state regime. This blue-shift is attributed to the loss of J-dimers during shearing,

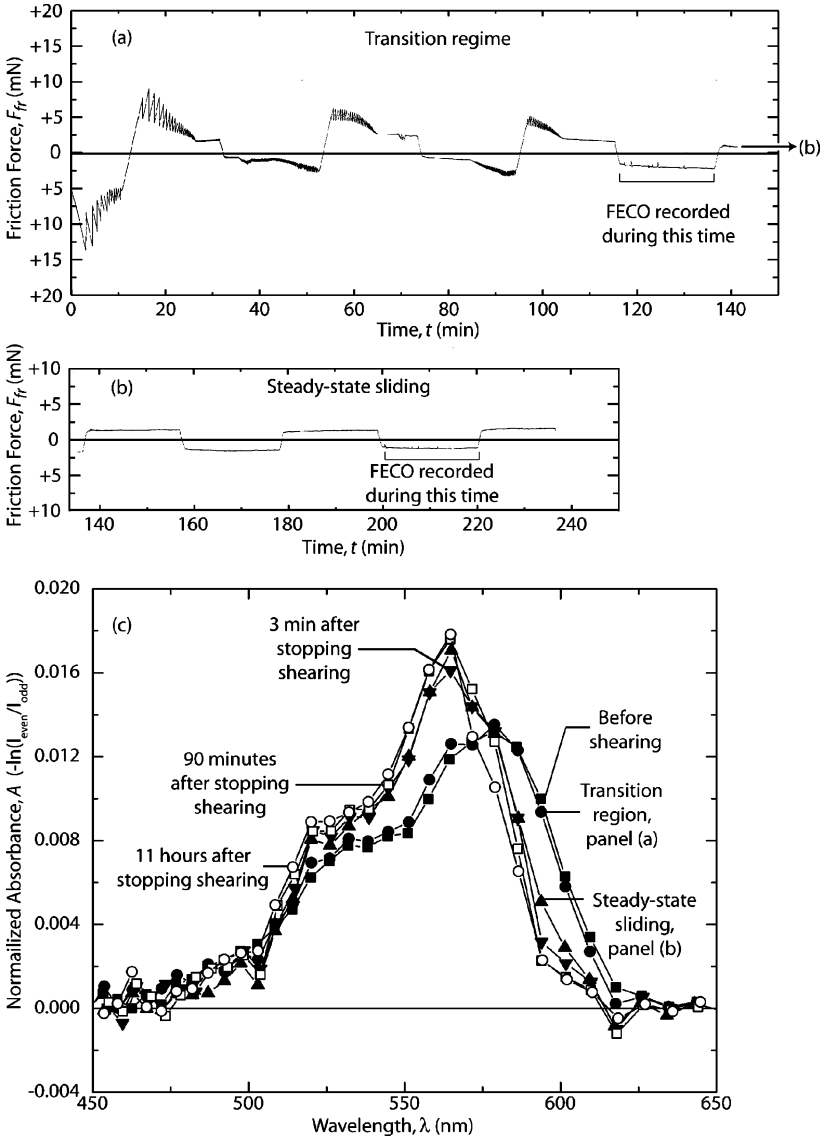

Figure 11. **(a)** Friction traces showing the "transition regime" during back and forth shearing at 0.08 μm/s over a distance of 100 μm of an initially 9 nm thick film of a 10 mM solution of RhB in 95:5 H_2O/EG. **(b)** Friction trace showing the steady-state regime during shearing as in part a. **(c)** Normalized absorbance spectra of the confined film obtained from the FECO recorded at the times shown in parts a and b as well as before and after shearing.

consistent with the previous findings. The lateral force due to shearing might have been strong enough to break apart the oblique configuration, favoring the monomer configuration. The blue shift is clearly not due to a temperature increase, as in Figure 2d, since the spectra remained unchanged 11 h after stopping shearing.

IV. Conclusions

Our results reveal that highly complex structural rearrangements can occur in two-component films when confined and sheared, involving different length and time scales. We chose rhodamine B because of its high absorbance and because its absorbance spectra depends on the configuration and orientation of these molecules. However, the results were so complex that they are open to a number of interpretations. Thus, many of our conclusions are qualitative rather than quantitative.

First, as solute molecules in solution, RhB initially adsorbs to mica surfaces even before they are brought together, resulting in a diffuse layer of varying (decreasing) density away from a surface. The adsorbed layers appear to exhibit both in-plane and out-of-plane heterogeneities, and appear to be composed of rhodamine nanoaggregates, mainly in the J-dimer configuration.

Simple confinement, i.e., without shear, changes the orientation of the adsorbed species, increasing the proportion of H-dimers, but also producing new molecular configurations (for example, linear aggregates that are not seen either in solution or on the isolated surfaces, but that have been theoretically predicted).

New rearrangements occur during shear. These can be slow to develop and may depend on the distance sheared rather than the shearing time.[80−82] The most dramatic effect is the nucleation of prismatic- or ribbon-shaped crystals of solid rhodamine B, manifested by a local increase in absorbance and easily visualized crystals inside the contact area (Figure 9). The thick crystals were concentrated near the center of the contact area and appeared to grow (nucleate) along the sliding direction. This suggests that in this case the nucleation is induced by pressure and shear, in contrast to the observed off-axis nucleation of molecularly thin hydrocarbon ribbons[51] that suggested a more

important role of epitaxial interactions of the hydrocarbon molecules with the surface lattice directions of the confining surfaces.

All of these effects occur at different regions rather than uniformly within the circular contact area. The reasons for this are (1) under static confinement the pressure is highest at the center and varies parabolically toward the circular boundary (cf. Hertz theory[83,84]), which can affect both the configuration and dynamics of trapped molecules;[78,79] (2) when two surfaces that have adsorbed layers on them are brought together, depending on the viscosity of the films and the approach rate, the surface deformations result in films of nonuniform thickness. The central regions can be thicker than those at the edges (cf. Figure 8), which further complicates the pressure distribution within the contact area. Shearing introduces additional nonuniform stresses even if the surface geometry is symmetrical. Thus, as one surface slides across the other the back and front ends of the film have different stress and alignment histories that depend on the shearing amplitude and the sliding velocity or shear rate.[81,82,85]

If the results of this study with rhodamine B apply to other confined systems, and there is no reason to believe that they should not, we may conclude that the molecules in confined and sheared films can undergo very complex structural changes occurring over different length scales (different short- and long-range order within the film), and different relaxation/adaptation times at different locations within an apparently uniform contact region. Finally, linear dye molecules, rather than the almost spherical rhodamine B, should be better suited for determining the effects of flow and shear on molecular alignment at or between two surfaces. Of particular interest would be the competing effects (on alignment) of shear and molecule−surface interactions.[51,77]

Acknowledgment. The authors thank the Zasadzinski lab for the use of their spectrophotometer. This work was supported by ONR Grant N00014-05-1-0540.

References and Notes

(1) López Arbeloa, F.; Ruiz Ojeda, P.; López Arbeloa, I. *Chem. Phys. Lett.* **1988**, *148*, 253.
(2) López Arbeloa, I.; Ruiz Ojeda, P. *Chem. Phys. Lett.* **1981**, *79*, 347.
(3) López Arbeloa, I.; Ruiz Ojeda, P. *Chem. Phys. Lett.* **1982**, *87*, 556.
(4) López Arbeloa, I.; Rohatgi-Mukherjee, K. K. *Chem. Phys. Lett.* **1986**, *128*, 474.
(5) Chambers, R. W.; Kajiwara, T.; Kearns, D. R. *J. Phys. Chem.* **1974**, *78*, 380.
(6) Chang, T.-L.; Cheung, H. C. *J. Phys. Chem.* **1992**, *96*, 4874.
(7) Faraggi, M.; Peretz, P.; Rosenthal, I.; Weinraub, D. *Chem. Phys. Lett.* **1984**, *103*, 310.
(8) Ferguson, J.; Mau, A. W. H. *Chem. Phys. Lett.* **1972**, *17*, 543.
(9) Muto, J. I. *Keio Eng. Rep.* **1972**, *25*, 71.
(10) Nishikiori, H.; Fujii, T. *J. Phys. Chem. B* **1997**, *101*, 3680.
(11) Ramette, R. W.; Sandell, E. B. *J. Am. Chem. Soc.* **1956**, *78*, 4872.
(12) Wong, M. M.; Schelly, Z. A. *J. Phys. Chem.* **1974**, *78*, 1891.
(13) Ali, M. A.; Moghaddasi, J.; Ahmed, S. A. *J. Opt. Soc. Am. B* **1991**, *8*, 1807.
(14) López Arbeloa, F.; Urrecha Aguirresacona, I.; López Arbeloa, I. *Chem. Phys.* **1989**, *130*, 371.
(15) Förster, T.; Konig, E. *Z. Elektrochem.* **1957**, *61*, 344.
(16) Gál, M. E.; Kelly, G. R.; Kurucsev, T. *J. Chem. Soc., Faraday Trans. 2* **1973**, *69*, 395.
(17) Kasha, M.; Rawls, H. R.; El-Bayoumi, M. A. *Pure Appl. Phys.* **1965**, *11*, 371.
(18) McRae, E. G.; Kasha, M. The molecular exction model. In *Physical Processes in Radiation Biology*; Augenstein, L., Mason, R., Rosenberg, B., Eds.; Academic Press: New York, 1964; p 17.
(19) Muto, J. I. *J. Phys. Chem.* **1976**, *80*, 1342.
(20) Rohatgi, K. K.; Singhal, G. S. *J. Phys. Chem.* **1966**, *70*, 1695.
(21) Selwyn, J. E.; Steinfeld, J. I. *J. Phys. Chem.* **1972**, *76*, 762.
(22) Smirl, A. L.; Clark, J. B.; Van Stryland, E. W.; Russell, B. R. *J. Chem. Phys.* **1982**, *77*, 631.
(23) Valdes-Aguilera, O.; Neckers, D. C. *Acc. Chem. Res.* **1989**, *22*, 171.
(24) Bojarski, P.; Jankowicz, A. *J. Lumin.* **1999**, *81*, 21.
(25) López Arbeloa, I.; Rohatgi-Mukherjee, K. K. *Chem. Phys. Lett.* **1986**, *129*, 607.
(26) Drexhage, K. H. Structure and Properties of Laser Dyes. In *Dye Lasers*; Schäfer, F. P., Ed.; Springer-Verlag: Berlin, 1973; p 144.
(27) Mulder, B. J. *Philips Res. Rep.* **1967**, *22*, 553.
(28) Mächtle, P.; Müller, C.; Helm, C. A. *J. Phys. II* **1994**, *4*, 481.
(29) Spitler, M.; Calvin, M. *J. Chem. Phys.* **1977**, *67*, 5193.
(30) Vuorimaa, E.; Ikonen, M.; Lemmetyinen, H. *Thin Solid Films* **1992**, *214*, 243.
(31) López Arbeloa, F.; Ruiz Ojeda, P.; López Arbeloa, I. *J. Lumin.* **1989**, *44*, 105.
(32) Nakashima, N.; Yoshihara, K.; Willig, F. *J. Chem. Phys.* **1980**, *73*, 3553.
(33) Porter, G.; Sadkowski, P. J.; Tredwell, C. J. *Chem. Phys. Lett.* **1977**, *49*, 416.
(34) Porter, G.; Tredwell, C. J. *Chem. Phys. Lett.* **1978**, *56*, 278.
(35) Kemnitz, K.; Yoshihara, K. *J. Phys. Chem.* **1991**, *95*, 6095.
(36) Fujii, T.; Nishikiori, H.; Tamura, T. *Chem. Phys. Lett.* **1995**, *233*, 424.
(37) Kemnitz, K.; Tamai, N.; Yamazaki, I.; Nakashima, N.; Yoshihara, K. *J. Phys. Chem.* **1986**, *90*, 5094.
(38) del Monte, F.; Levy, D. *J. Phys. Chem. B* **1998**, *102*, 8036.
(39) del Monte, F.; Mackenzie, J. D.; Levy, D. *Langmuir* **2000**, *16*, 7377.
(40) Klika, Z.; Weissmannová, H.; Capková, P.; Pospíšil, M. *J. Colloid Interface Sci.* **2004**, *275*, 243.
(41) Pospíšil, M.; Capková, P.; Weissmannová, H.; Klika, Z.; Trchová, M.; Chmielová, M.; Weiss, Z. *J. Mol. Model.* **2003**, *9*, 39.
(42) Kasha, M. Molecular excitons in small aggregates. In *Spectroscopy of the excited state*; Bartolo, B. D., Ed.; Plenum Press: New York, 1976; p 337.
(43) The "linear" dimer structure is theoretically possible, but to our knowledge it has not been experimentally observed for the rhodamine B dye.
(44) Kajiwara, T.; Chambers, R. W.; Kearns, D. R. *Chem. Phys. Lett.* **1973**, *22*, 37.
(45) Bojarski, P.; Matczuk, A.; Bojarski, C.; Kawski, A.; Kuklinski, B.; Zurkowska, G.; Diehl, H. *Chem. Phys.* **1996**, *210*, 485.
(46) López Arbeloa, F.; Chaudhuri, R.; Arbeloa López, T.; López Arbeloa, I. *J. Colloid Interface Sci.* **2002**, *246*, 281.
(47) Humpolícková, J.; Procházka, K.; Hof, M. *Coll. Czech. Chem. Commun.* **2003**, *68*, 2105.
(48) Speas, W. E. *Phys. Rev.* **1928**, *31*, 569.
(49) Xie, H.; Song, K.; Mann, D. J.; Hase, W. L. *Phys. Chem. Chem. Phys.* **2002**, *4*, 5377.
(50) Landman, U.; Luedtke, W. D.; Ringer, E. M. Molecular dynamics simulations of adhesive contact formation and friction. In *Fundamentals of Friction: Macroscopic and Microscopic Processes*; Singer, I. L., Pollack, H. M., Eds.; Kluwer Academic Publishers: Dordrecht, Netherlands, 1992; p 463.
(51) Drummond, C.; Alcantar, N.; Israelachvili, J. *Phys. Rev. E* **2002**, *66*, 011705.
(52) Israelachvili, J. N.; McGuiggan, P. M. *J. Mater. Res.* **1990**, *5*, 2223.
(53) Israelachvili, J. N. *J. Colloid Interface Sci.* **1973**, *44*, 259.
(54) Heuberger, M.; Luengo, G.; Israelachvili, J. *Langmuir* **1997**, *13*, 3839.
(55) Homola, A. M.; Israelachvili, J. N.; Gee, M. L.; McGuiggan, P. M. *J. Tribol.* **1989**, *111*, 675.
(56) Luengo, G.; Schmitt, F.-J.; Hill, R.; Israelachvili, J. *Macromolecules* **1997**, *30*, 2482.
(57) Müller, C.; Mächtle, P.; Helm, C. A. *J. Phys. Chem.* **1994**, *98*, 11119.
(58) Bergmann, K.; O'Konski, C. T. *J. Phys. Chem.* **1963**, *67*, 2169.
(59) Grünewald, T.; Dähne, L.; Helm, C. A. *J. Phys. Chem. B* **1998**, *102*, 4988.
(60) Grauer, Z.; Malter, A. B.; Yariv, S.; Avnir, D. *Colloids Surf.* **1987**, *25*, 41.
(61) Grauer, Z.; Avnir, D.; Yariv, S. *Can. J. Chem.* **1984**, *62*, 1889.
(62) Tapia Estévez, M. J.; López Arbeloa, F.; López Arbeloa, T.; López Arbeloa, I. *Langmuir* **1993**, *9*, 3629.
(63) Tapia Estévez, M. J.; López Arbeloa, F.; López Arbeloa, T.; López Arbeloa, I.; Schoonheydt, R. A. *Clay Miner.* **1994**, *29*, 105.
(64) Tapia Estévez, M. J.; López Arbeloa, F.; López Arbeloa, T.; López Arbeloa, I. *J. Colloid Interface Sci.* **1995**, *171*, 439.
(65) Chaudhuri, R.; Arbeloa, F. L.; Arbeloa, I. L. *Langmuir* **2000**, *16*, 1285.
(66) López Arbeloa, F.; Herrán Martínez, J. M.; López Arbeloa, T.; López Arbeloa, I. *Langmuir* **1998**, *14*, 4566.

(67) Sasai, R.; Fujita, T.; Iyi, N.; Itoh, H.; Takagi, K. *Langmuir* **2002**, *18*, 6578.
(68) Matsuo, Y.; Fukutsuka, T.; Sugie, Y. *Chem. Lett.* **2003**, *32*, 1004.
(69) Capková, P.; Malý, P.; Pospíšil, M.; Klika, Z.; Weissmannová, H.; Weiss, Z. *J. Colloid Interface Sci* **2004**, *277*, 128.
(70) Capková, P.; Pospíšil, M.; Weiss, Z. *J. Mol. Model.* **2003**, *9*, 195.
(71) Yariv, S. *Int. J. Trop. Agric.* **1988**, *6*, 1.
(72) Vyshkvarko, A. A.; Kiselev, V. F.; Paschenko, V. Z.; Plotnikov, G. S. *J. Lumin.* **1991**, *47*, 327.
(73) Liang, Y.; Moy, P. F.; Poole, J. A.; Goncalves, A. M. P. *J. Phys. Chem.* **1984**, *88*, 2451.
(74) Nishikiori, H.; Tanaka, N.; Fujii, T. *Res. Chem. Intermed.* **2000**, *26*, 469.
(75) Killesreiter, H. *Ber. Bunsen—Ges. Phys. Chem.* **1978**, *82*, 503.
(76) Blomberg, E.; Claesson, P. M.; Christenson, H. K. *J. Colloid Interface Sci.* **1990**, *138*, 291.
(77) Akbulut, M.; Chen, N.; Maeda, N.; Israelachvili, J.; Grunewald, T.; Helm, C. *J. Phys. Chem. B* **2005**, *109*, 12509.
(78) Mukhopadhyay, A.; Zhao, J.; Bae, S. C.; Granick, S. *Phys. Rev. Lett.* **2002**, *89*.
(79) Mukhopadhyay, A.; Zhao, J.; Bae, S. C.; Granick, S. *Rev. Sci. Instrum.* **2003**, *74*, 3067.
(80) Israelachvili, J.; Giasson, S.; Kuhl, T.; Drummond, C.; Berman, A.; Luengo, G.; Pan, J.-M.; Heuberger, M.; Ducker, W.; Alcantar, N. *Tribol. Ser.* **2000**, *38*, 3.
(81) Drummond, C.; Israelachvili, J. *Phys. Rev. E* **2001**, *63*, 041506.
(82) Drummond, C.; Israelachvili, J. *Macromolecules* **2000**, *33*, 4910.
(83) Israelachvili, J. *Intermolecular and surface forces*, 2nd ed.; Academic Press: San Diego, 1992.
(84) Hertz, H. *J. Reine Angew. Math.* **1881**, *92*, 156.
(85) Dhinojwala, A.; Cai, L.; Granick, S. *Langmuir* **1996**, *12*, 4537.